2023

Temperature and H2O Species Measurements Via a Laser Spectroscopic Sensor in Harsh Reacting Environments

Marc B. Etienne
University of Central Florida

TEMPERATURE AND H_2O SPECIES MEASUREMENTS VIA A LASER SPECTROSCOPIC SENSOR IN HARSH REACTING ENVIRONMENTS

by

MARC B. ETIENNE

B.S University of Central Florida, 2021

A thesis submitted in partial fulfillment of the requirements
for the degree of Master of Science
in the Department of Mechanical and Aerospace Engineering
in the College of Engineering and Computer Science
at the University of Central Florida
Orlando, Florida

Fall Term
2023

ABSTRACT

Reactive material liners paired with high explosives can significantly increase blast effects. This research aims to study the properties that primarily control the interaction between reactive materials (RM) and high explosives (HE). This will facilitate blast performance optimization for the RM and HE combinations. A laser spectroscopic sensor will be utilized to measure the performance of these RM and HE combinations. Laser absorption spectroscopy (LAS) is a technique that measures the chemical concentration of a medium through the intensity change of the laser beam. The laser diagnostic instrument is composed of two tunable diode lasers, one centered at 2.48 μm and the other at 2.55 μm. The sensor is designed to measure H_2O species concentration in the blast wave using the beer-lambert law. It will also measure the temperature of the blast with a high temperature sensitivity in the 1000 K to 2600 K range. The temperature and concentration data will be used to assess the combustion performance of the blast. The data was collected at a 200 MHz sampling frequency through a fiber-coupled optical probe designed to shield the sensitive optical equipment. The resulting blast temperature and molar concentration of H_2O will be used to determine the optimal RM liner and HE pairings in the MMRT chamber. This research will enable the AFRL to expand their understanding of the RM and HE pairings.

ACKNOWLEDGMENTS

I would like to thank my advisor Dr. Subith Vasu for allowing me to pursue my master's degree. I would like to thank my teammates Nishan Khanal, Robert Greene, and Andrew Derusha for their support and help in conducting this project. Their unique skills and experiences were paramount in helping to design the laser sensor, data acquisition system, and data processing code. I would also like to thank Dr. Erik Ninnemann and Dr. Justin Urso who were great resources for building this diagnostic instrument. Special thanks to James Essad who was essential in machining the optical probe. This research would not be possible without the support of the U.S. Air Force Research Laboratory (AFRL) (FA8651-18-2-0005). This work is also made possible by partial funding from AFOSR (FA9550-20-1-0268), NASA (80NSSC21M0308), the University of Central Florida (UCF), and the Florida High Tech Corridor Council (FHTCC). Lastly, I would like to thank my family and friends, they were pillars that continuously kept pushing me to complete my master's degree.

TABLE OF CONTENT

LIST OF FIGURES

1. INTRODUCTION

1.1 Reactive Materials and High Explosives

Reactive materials (RM) are a new class of energetic materials that are currently being studied for military applications. These materials stay inert until subjected to a strong stimulus, then they undergo a fast-burning process and release a high level of kinetic and chemical energy. Due to their unique properties, they greatly enhance the lethal blast effects of warheads [1]. They can be applied to different weapons concepts by enhancing different components of the warhead. A penetrating warhead can be enhanced by replacing some of the inert parts of the warhead with reactive materials [1]. RM are different from traditional energetic materials such as explosives and propellants.

High explosives (HE) are simply explosives that undergo a detonation process. In a high-explosive process, initiators are used in the primary composition to initiate the detonation process. Bursting charge explosives are then used to increase the detonation strength [2]. HE have a property called brisance. This shattering capability of HE makes them very valuable for military applications. This study aims to determine the pairings of RM and HE that will result in greatly increasing the blast effects. To characterize the effects of the RM and HE combinations, laser absorption spectroscopy is used to determine the chemical properties of the blast. This is because it is a non-intrusive method of recording the chemical properties of a combustion event [3]. It can also retrieve a very accurate time-resolved measurement of the combustion chemistry.

1.2 Background on Laser Absorption Spectroscopy

Laser absorption spectroscopy (LAS) is a technique that uses a laser to measure the chemical concentration in a medium. This is done by measuring the change in intensity of the laser [4-9]. Using the beer-lambert law, the absorption of the laser can be calculated. The measured absorption can be used to calculate temperature and chemical concentration. LAS can be used to measure the combustion properties in a variety of flow fields. This includes shock tubes, detonation tubes, combustion chambers, and rotating detonation engines. C. S. Goldenstein et al. measured the temperature and water concentration in a rotating detonation engine [10]. Recent research in LAS have moved towards using tunable diode lasers, which are semiconductor lasers. They are great for continuous wave lasing applications because they provide very stable wavelengths. Tunable diode lasers provide a broad range of spectral line selections.

Tunable diode lasers' inherent properties make them great options for LAS. Numerous techniques are used in LAS. There are several advantages and disadvantages to these strategies; Baer et al. and Rieker cover some of these strategies in great detail [4] [11]. For this research effort, the fixed-wavelength laser absorption spectroscopy (FW-LAS) technique was chosen. This is because of its simplicity and high acquisition rate. Being that reactive materials are a relatively new research field, there are lots of experiments that can be done to improve the foundational knowledge on these materials. This research effort will focus on determining the temperature and molar fraction of water in the reactive material and high explosive blast using LAS. This will assess the combustion performance of the blast.

2. THEORY

2.1 Fixed Wavelength Absorption Spectroscopy

One of the most important relations in LAS is the beer-lambert law [12]. This law relates the change in signal intensity to absorbance. It can be summarized as:

$$\alpha = -\ln\left(\frac{I}{I_0}\right)_\lambda = \sigma(\lambda, P, T)\frac{P}{R_u T}xL \quad (1)$$

Here α is the absorbance, I is the transmitted intensity, I_0 is the reference intensity, σ is the cross-sectional absorbance, λ is the wavelength, P is the pressure, T is the temperature, R_u is the gas constant, x is the species concentration, and L is the pathlength. The change in laser intensity is used to calculate the absorbance of the spectral line. As shown in Equation 1, absorbance can also be related to the temperature and species concentration. As mentioned earlier, FW-LAS was chosen due to several factors. It has very fast acquisition rates, typically you are only limited by the data acquisition system [4]. It is very simple to set up since it needs very minimal electronic hardware. For example, FW-LAS does not require a function generator to modulate the laser. Unfortunately, this technique does have some drawback. One of the main disadvantages to utilizing this technique is that it inherently has a high uncertainty in the wavelength. This can be mitigated by monitoring the laser's wavelength throughout the experiment using a wavelength analyzer.

2.2 Temperature and Mole Fraction Determination

Laser pyrometry related the change in the intensity of emitted light to the change in the temperature of the source [13]. There are several methods to retrieve the temperature using laser pyrometry. The method that was selected for this research effort is two-line laser pyrometry. These lines must measure the same species, and ideally, are narrow bands. These two spectral lines must

have different temperature sensitivities. One line will be more sensitive at lower temperatures and the other at higher temperatures. The broadening effects due to temperature and pressure must also be considered when selecting these two line pairs. Once the ideal line pairs are determined the ratio of their absorbance can be compared to the ratio of the cross-sectional absorbance.

$$B(P,T,\lambda) = \frac{\alpha_1}{\alpha_2} = \frac{\sigma_1(P,T,\lambda)}{\sigma_2(P,T,\lambda)} \quad (2)$$

Equation 2 demonstrates the process behind the calculation for temperature. B is the absorbance ratio, α_1, σ_1, α_2, and σ_2 are the absorbance and cross-sectional absorbance for the first and second spectral lines, respectively. Several researchers use the HITEMP and HITRAN databases to simulate the absorption cross-section for their targeted spectral lines [14]. The absorption cross-section can be simulated at different temperature and pressure points. Once the absorbances of both lasers are determined from the measured change in laser intensity, their ratio and the experimentally measured pressure can be taken to calculate temperature.

2.3 Line Selection and Temperature Sensitivity

There are several parameters that are necessary to consider when selecting the spectral lines. The lines must have adequate absorbance over the expected temperature range. The peak absorbance of the transition can be calculated using Equation 3.

$$\alpha_{v,peak} = S_i(T)\, P\, x_{H_2O}\, L\phi_{v,peak} \quad (3)$$

In this equation, P is the static pressure in atm, $S_i(T)$ is the line strength in cm^{-2} atm^{-1}, L is the pathlength in cm, x is the mole fraction, and $\phi_{v,peak}$ is the line-shape function peak value [15]. Using this peak absorbance equation, the minimum detectable absorbance can be determined. The line strength ratio of the two transitions should ideally be within the R = 0.2 to 5 range. The adverse

effects from wing of the stronger transition on the weaker transition can be mitigated within this range. The two lines should have suffciently different lower state energies E" [15].

$$|\Delta E_i^{"}| = \left|E_1^{"} - E_2^{"}\right| \geq \left|\frac{dR/R}{dT/T}\right| T \ \frac{k}{hc} \tag{4}$$

$$\sigma_T = \left|\frac{dR/R}{dT/T}\right| \tag{5}$$

Here, k is Bolzmann's constant, h is Plank's constant, c is the speed of light, T is temperature, and σ_T is the temperature sensitivity. Lastly, the selected lines must also be well isolated from any significant interfering transitions. From these parameters, it was determined that the spectral lines shown in Figure 1 would be the most effective for this water characterization effort. As they are mid-infrared transitions, they have very strong absorption features. Since the 3920.089 cm^{-1} transition has a lower state energy of 704.2 cm^{-1}, and the 4029.524 cm^{-1} transition has a lower state energy of 2660.95 cm^{-1}, these lines have an adequately different lower state energy. The temperature sensitivity for these lines is plotted in Figure 2. Lastly, they are also not expected to significantly absorb any other major species that are predicted to form in the detonative flow field based on spectral analysis from the HITEMP and HITRAN database.

A.

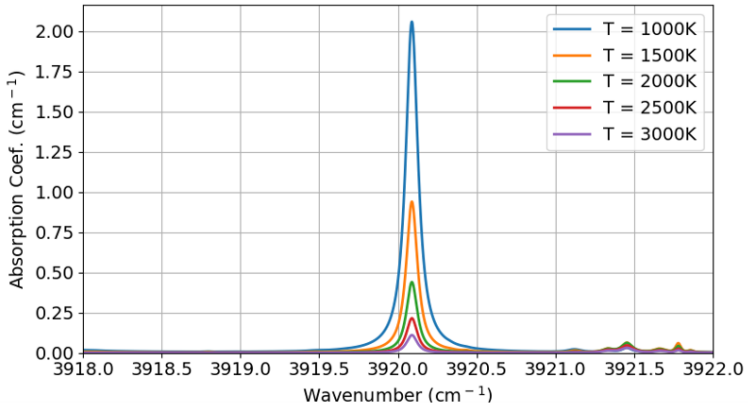

B.

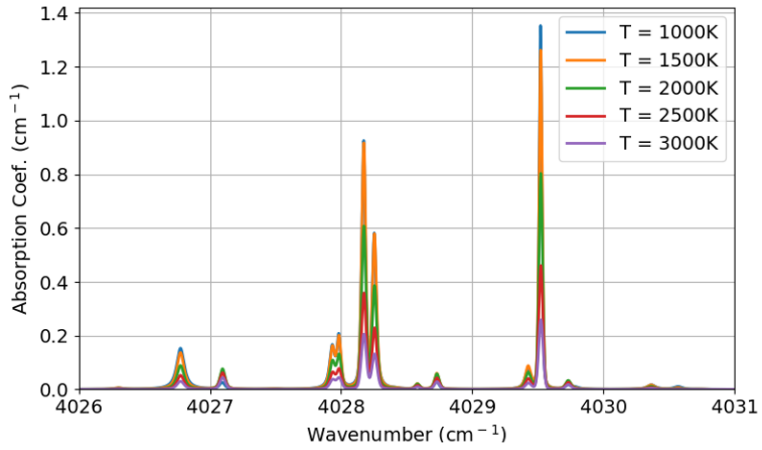

Figure 1: a.) 3920.089 cm-1 spectral line, and b.) 4029.524 spectral line.

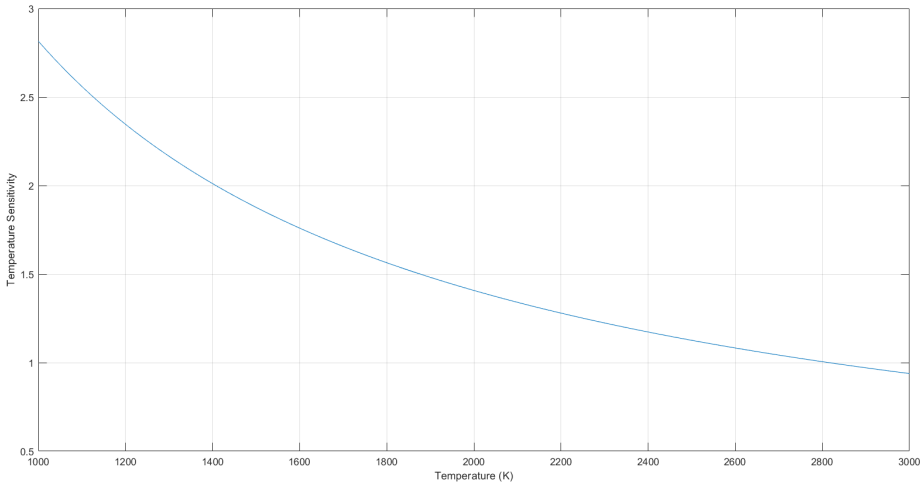

Figure 2: Temperature sensitivity distribution from 1000 K to 3000 K.

3. EXPERIMENTAL METHODS

3.1 Laser Diagnostic Instrument

Figure 3 shows the schematic of the diagnostic instrument that was used for the absorption experiment. The diagnostic instrument utilizes two distributed feedback (DFB) tunable diode lasers that are designed to measure H_2O. The first laser is centered at 2.481 µm with a targeted spectral line of 4029.524 cm^{-1} and the second laser is centered 2.551 µm laser with a targeted

spectral line of 3920.089 cm^{-1}. Both lasers are class 1M nanoplus lasers. The 2.48 μm laser and the 2.55 μm laser has a power output of 11 mW and 10 mW respectively. The 4029.524 cm^{-1} spectral line is more sensitive at higher temperatures compared to the 3920.089 cm^{-1} line. The combination of these two lines results in a greater than nominal temperature sensitivity in the range of 1000 K to 2800 K. The lasers and all the optical components are incased in two acrylic boxes as depicted in the schematic. Both boxes are purged with nitrogen to lower the humidity level in the boxes. This is to mitigate the atmospheric absorption of the lasers. The lasers are made colinear through a 50 – 50 beam splitter in the pitch box. The pitch box has two main paths: a reference path and a transmitted path. The reference path has another 50 – 50 beam splitter that divides the colinear beams into two different paths. The lasers travel through the first path to a 3.5 μm grating (GR2550-30035), where they are separated and sent to their respective reference detectors. The second path sends the beams to a spectrum analyzer (Bristol 771B-MIR). The Bristol allows us to confirm that the lasers remain on peak throughout the experiment.

In the transmitted path, the lasers travel through a reflective collimator (RC02SMA-P01) and then through the 1st optical fiber. They are sent through the MMRT structure, caught by a second optical fiber, and sent to the catch box using another reflective collimator. The first fiber (MF21L2) has a core diameter of 200 μm, but the second (MF11L2) has a 100 μm diameter. The second fiber is used on the catch box particularly because of its smaller diameter. From experimentation, it was determined that the 100 μm fiber will provide a better separation of the two beams in the catch box. The catch box utilizes a 3.1μm diffraction grating (GR2550-45031) to separate the lasers and send them to their respective detectors. This grating provides a greater reflected beam intensity and larger separation angle compared to the 3.5 μm grating. The laser setup contains a total of four photovoltaic mid-IR detectors. Two of which are in the pitch box (reference detectors) and the

other two are in the catch box (transmitted detectors). Two PVI-4TE-3-2x2 and two PVI-2TE-3.4 photovoltaic detectors were used to measure the 2.48 µm laser and the 2.55 µm laser respectively.

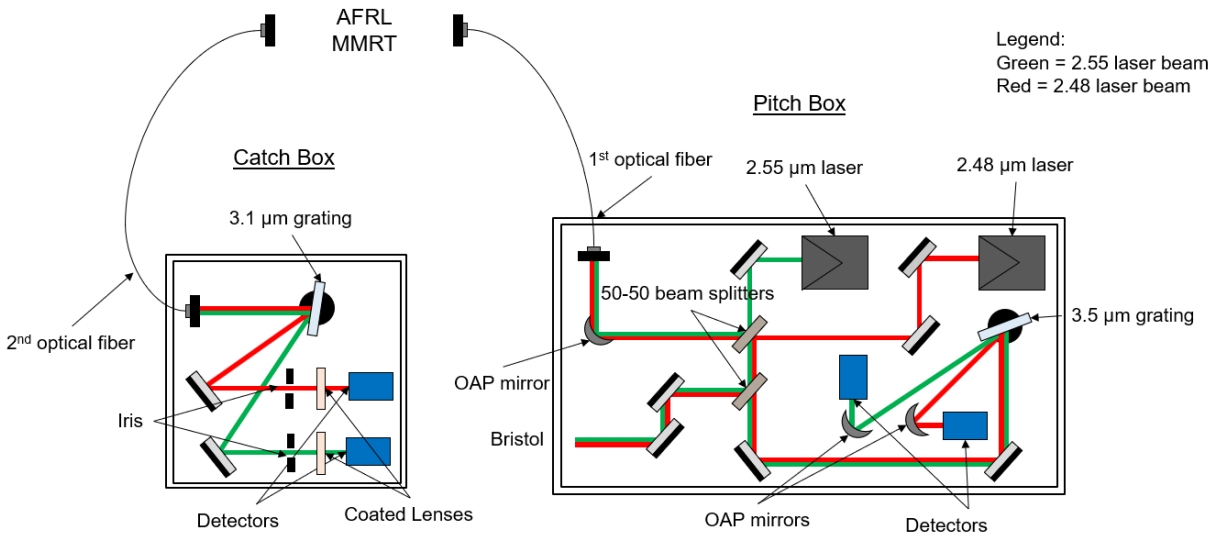

Figure 3: Diagnostic Instrument and all the optical components within it.

3.2 Optical Probe

The lasers are pitched through the Augmented Modular Multi-Room Target (MMRT) structure via a fiber coupled optical probe with a pathlength of 4 Inches. Figure 4 shows the design concept of the probe as well as its components. The revealed side of the bottom plate is bolted and secured on the exterior wall of the MMRT structure. The MMRT structure can be seen in figure 13. The two chambers go through the cutout in the bottom plate and a similar sized cutout in the walls of the MMRT structure. This will be elaborated on further down. The probe was designed in this manner to allow the research team to quickly remove the probe and clean the windows on the chambers from test to test. This is an important feature to account for any sooth formation, or any particles or debris covering the windows since this will reduce and sometimes completely eliminate the lasers signals.

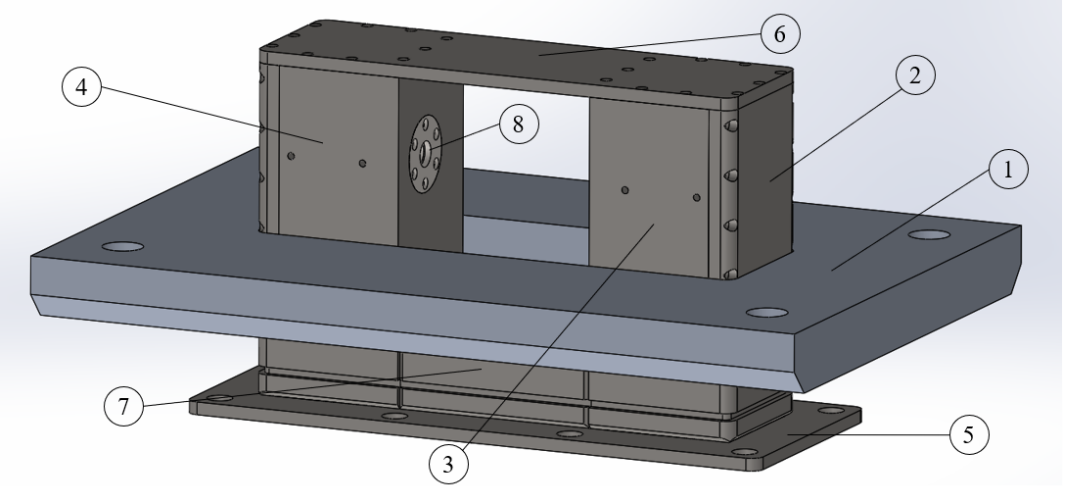

Part NO.	Part Name
1	Bottom Plate
2	Back Plate
3	Catch Chamber
4	Pitch Chamber
5	Support Plate
6	Top Plate
7	Wall thickness
8	Window holder

Figure 4: The MMRT Probe and its components.

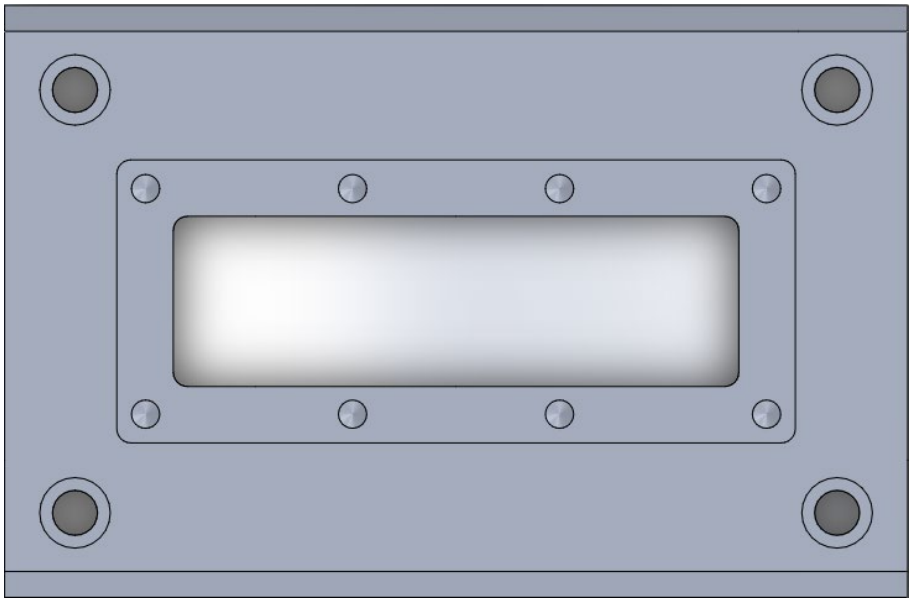

Figure 5: Top-down view of the bottom plate.

The bottom plate is the largest component of the optical probe. It is made entirely out of 6061 aluminum alloy. Figure 3 shows the hole cutouts in the bottom plate that will allow it to

interface with the remaining components of the probe as well as the MMRT chamber. Four bolts, nuts, and washers were used to secure the bottom plate directly to the MMRT chamber. These bolts were inserted through the four holes located at the corners of the bottom plate. The components of the probe that houses the optics will be inserted through the inner most rectangular cutout of the bottom plate. They will then travel through a similar sized cutout in the MMRT chamber. The eight smaller holes on the bottom plate are used to secure the support plate to the bottom plate. When setting up the probe, this will be the last step in the process.

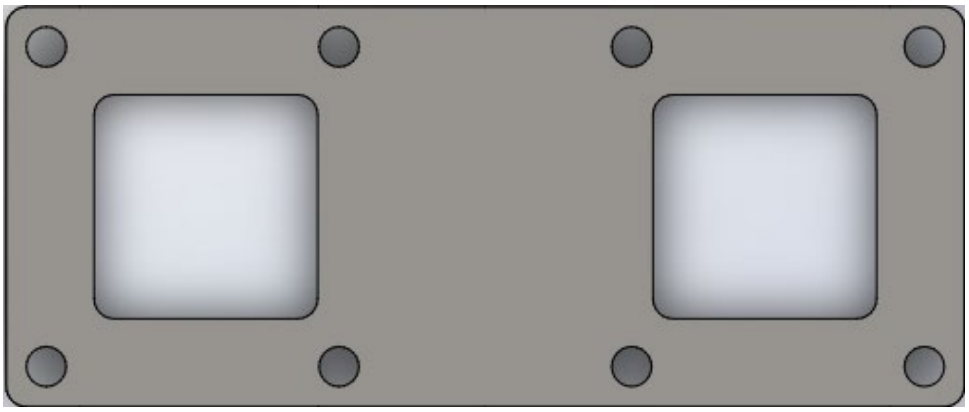

Figure 6: Top-down view of the support plate.

The support plate shown in Figure 6 is a critical component that supports the junction that fuses the main probe components. The main probe components consist of all the components listed in Figure 4 excluding the bottom plate. All the main probe components are made of 304 Stainless Steel. An important design concern for the selection of this material is the expected harsh environment in the MMRT chamber. All the main probe components excluding the support plate are directly exposed to this harsh environment. Stainless Steel was a good choice here because it will experience much lower deformation from the force of the blast wave compared to other

material choices such as aluminum. The Stainless-Steel frame will also mitigate the impact that any high-speed shrapnel could have on the optical equipment. The support plate, wall thickness, and pitch and catch chambers were designed to be welded together. Since it is better to weld similar materials together, Stainless Steel was chosen for all those components.

A. 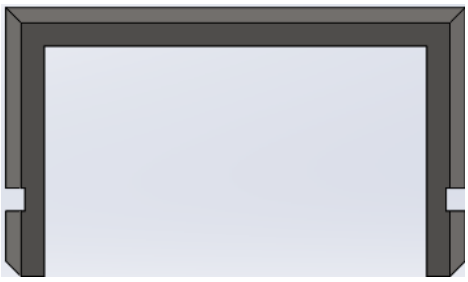 B. 

Figure 7: Side views of the wall thickness; a.) y-z plane view, b.) x-z plane view.

The wall thickness is the part shown in Figure 7. This rectangular part was cut into this shape in order to reduce the weigth of the probe. The wall thickness is designed to weld directly to the support plate, and the pitch and catch chambers. The sides of the wall thickness was fillet to facilitate the welding process. There is a groove on both sides of the piece for an O-ring to rest in. These O-ring grooves will connect to the O-ring grooves on the pitch and catch chambers. The O-ring grooves can be seen in Figure 8. Originally, these grooves were designed to prevent exposure of the support plate and weld to any particles. Although, these O-ring grooves were not utilized since exposure to any particles would be very brief and therefore would not have much of an impact on support plate.

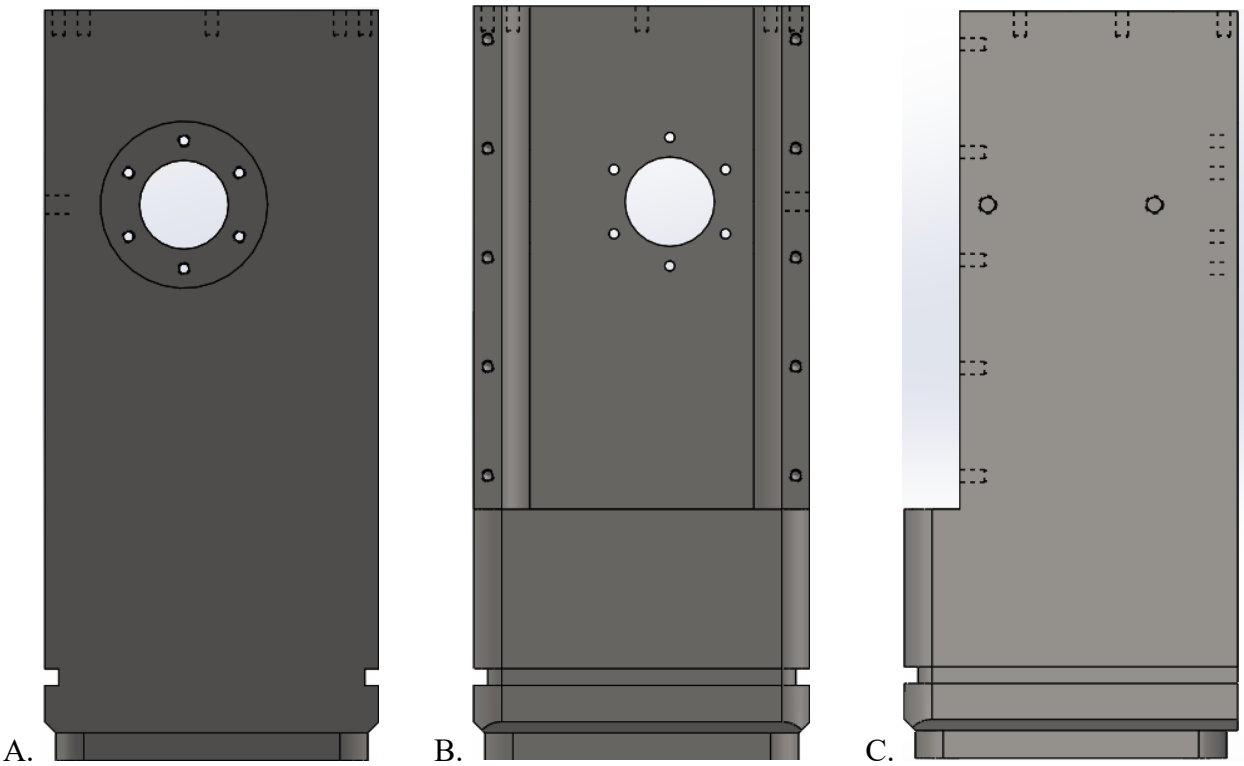

Figure 8: Pitch chamber of the optical probe; a.) Front view, b.) back view, c.) side view.

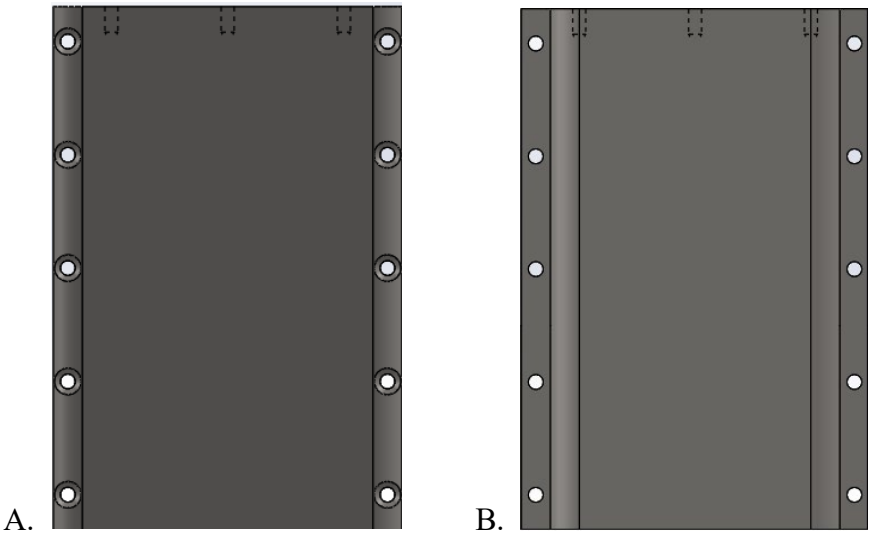

Figure 9: a.) front view of the back plate, b.) back view of the back plate.

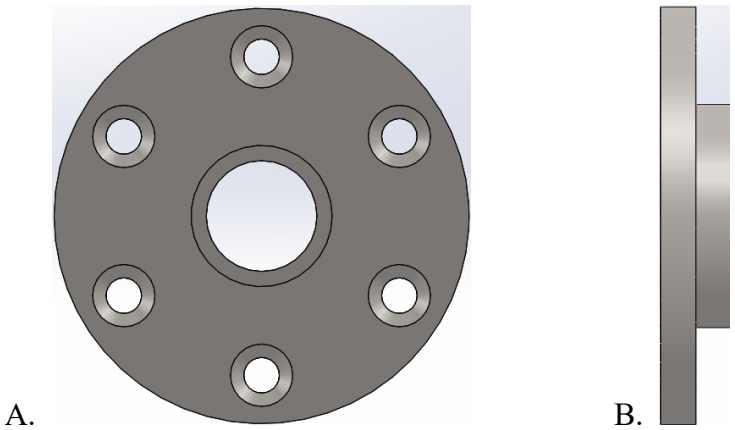

Figure 10: Optical probe window holder; a.) front view, b.) side view.

The pitch chamber is machined from a rectangular pipe. As shown in Figure 8, it is machined with several cuts. A circular cut on the front face that will be used to attach the window holder piece to the chamber, a cut at the back that is used to make the back plate, and a cut at the bottom of the structure that is used to weld the chamber to the support plate. The catch chamber is designed exactly the same as the pitch chamber, exept the window's and optical component's locations are symmetrically inverted about the horizontal center of the chambers. There is a total of two back plates, on for each chamber. The back plate has several screw holes on its face and on its top side that are used to secure the plate to the chamber and the top plate. There is also a total of two window holders. A window was glued to this piece using epoxy. The window is designed to rest inside the window holder. The window works really well for these mid-IR lasers as they transmitted the beams with minimal attenuation.

A.

B.

Figure 11: Top plate a.) bottom view, b.) front view.

A. B. C. D.

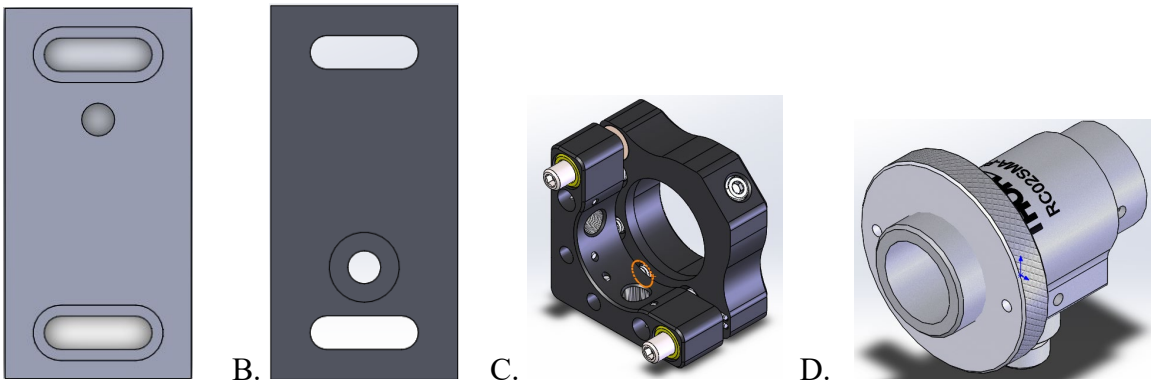

Figure 12: Optical components and fixture. A.) Top view of optics base, b.) bottom view of optics base, c.) half-inch diameter kinematic mirror mount, and d.) reflective collimator.

The pitch and catch chambers each houses an optics base, a kinematic mirror, and reflective collimators. The reflective collimator (RC02SMA-P01) and the half-inch kinematic mirror mount (KM05) were acquired from Thorlabs. To set the optical components for the probe, the reflective collimator is directly fastened to the kinematic mirror mount. The mirror mount is screwed to the optics base using the circular cutout shown in Figure 12 a and b. The straight slots are used to

secure the optics base to the side of the chambers. The hole that connects to these slots are shown in Figure 8 c. The optics base was design with these slots and not regular threated holes to allow the base to move and better align the reflective collimator to the window. Essentially, the thickness of the optics base accounts for the horizontal alignment of the collimator in respect to the chamber body. The slots on the optics base accounts for the vertical alignment of the collimator to the chamber's body. To further explain, in Figure 8 b, if the optical components were secured to the chamber, then the optics base would rest on the interior right wall of the chamber. The collimator would be horizontally centered to the window of the chamber, and using the slots, the collimator could also be vertically centered to the window.

The reflective collimators in both chambers are connected to the pitch and catch boxes through the use of fibers. Two optical fibers are utilized, the first is an MF21L2 fiber and the second is an MF11L2 fiber. Each of these fibers will go through one of the chambers and attach to the reflective collimator in that chamber. The laser beams will run through the first optical fiber in the pitch chamber and will then be sent through the window to the catch chamber via the reflective collimator. The beams will be received by the reflective collimator in the catch chamber and transmitted to the catch box through the second optical fiber. These sensitive optical components need to be protected from the negative impacts of the blasts produced in the MMRT structure. This was a top priority when designing this probe. As mentioned above, the probe was made from 304 stainless steel to reduce the detrimental effects of the harsh environment inside the MMRT structure. Also, both chambers have a seal system with Viton O-rings (9464K232) from McMaster-Carr to prevent any gas or particle leaking into the body. Any leaks could potentially damage the optical components and very likely interfere with the laser measurements. The O-ring groove for the seal system, as shown in Figure 11 b, is machined on the side of the top plate component.

3.3 MMRT chamber

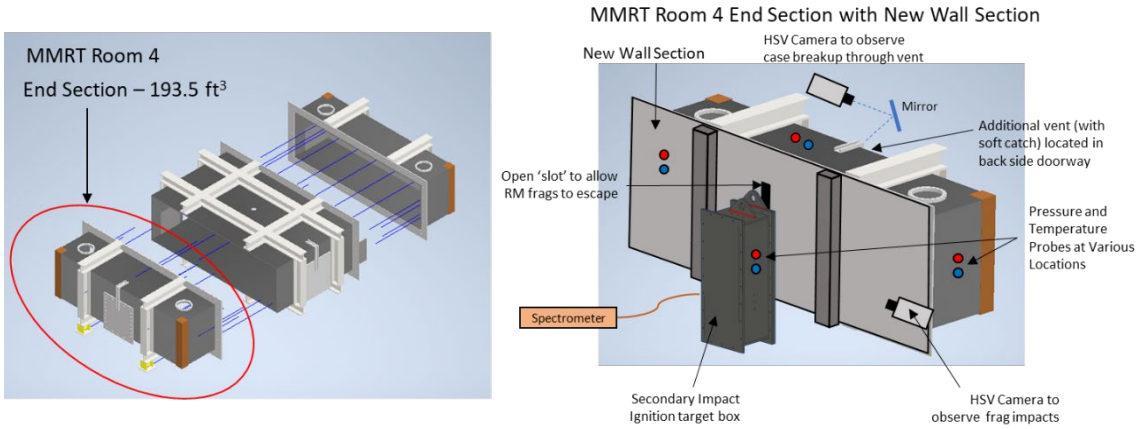

Figure 13: Schematic of the MMRT test structure.

The experiment is composed of 13 tests containing several changing parameters between tests. Although, all test items are detonated top-down with an RP series and Comp A-5 booster. The test items are suspended vertically and secured in the MMRT structure. This is to make sure that the center of the cylindrical test item is aligned directly under the hole on the roof of the test structure. The vertical center of the test item is adjusted to be two feet above the floor of the structure.

3.4 Data Collection

A four channels DAQ that is sampled at 200 MHz was used to collect the laser data. Due to the limited amount of channels on the DAQ, the 2.48 µm laser reference detector was replaced with a trigger signal. This will allow the LabVIEW software to start recording data at the exact moment of detonation. The reference detector measurement is important because it accounts for the power fluctuation of the laser during a test. Although, this was not necessary for the 2.48 µm

laser since it had very minimal power fluctuations. A zero, reference, and detonation measurement was taken for each test. The zero measurement provided a reference point for the signal bias on the detector. The reference measurement acted as a baseline signal for the lasers before the detonation event. Lastly, the detonation measurement is taken during the fire of the test item.

The change in intensity of both lasers were taken to calculate their respective absorbances using the beer-lambert law. Using the ratio of the absorbances of the two lasers, the temperature, and the species concentration was determined. For temperature calculation, the cross-sectional absorbance of water at 4029.524 cm^{-1} and 3920.089 cm^{-1} was simulated at different temperatures and pressures using the HITEMP database. The HITEMP database was validated for the targeted spectral lines through a characterization experiment using a shock tube. The pressure data for this experiment was provided by the Eglin team. The collected data was processed in MATLAB and smoothed using a Savitzky-Golay filter.

4. DATA ANALYSIS

4.1 Probe and Laser Results

This experiment returned several interesting findings. The first being the successes and failures of the probe. The probe provided a safe housing for the optical components, while also providing a way to clean the optical windows between tests. Although, there are considerable vibrational noises from the blast acting on the probe. This in turn transfer noticeable noise to the laser signals. The laser system appears to have a minimum temperature that it can detect from the blast. This is mainly due to the 2.48 µm laser, since it can only detect water when the blast temperature reaches the minimum temperature required for it to absorb. This can be seen by comparing the absorbance plots. In Figure 14, when taking the mean absorbance of the 2.48 µm laser, it can be seen that this laser is not absorbing. This is not the case in Figure 15, where the absorption of the 2.48 µm laser is comparable to the absorption of the 2.55 µm laser.

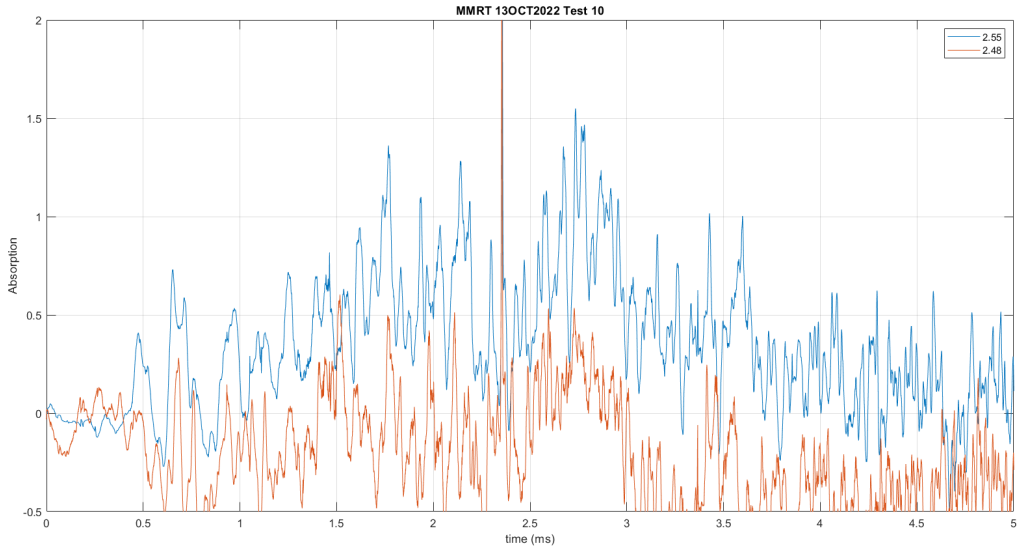

Figure 14: Absorbance trace of both H_2O lasers for test 10 of the experiment.

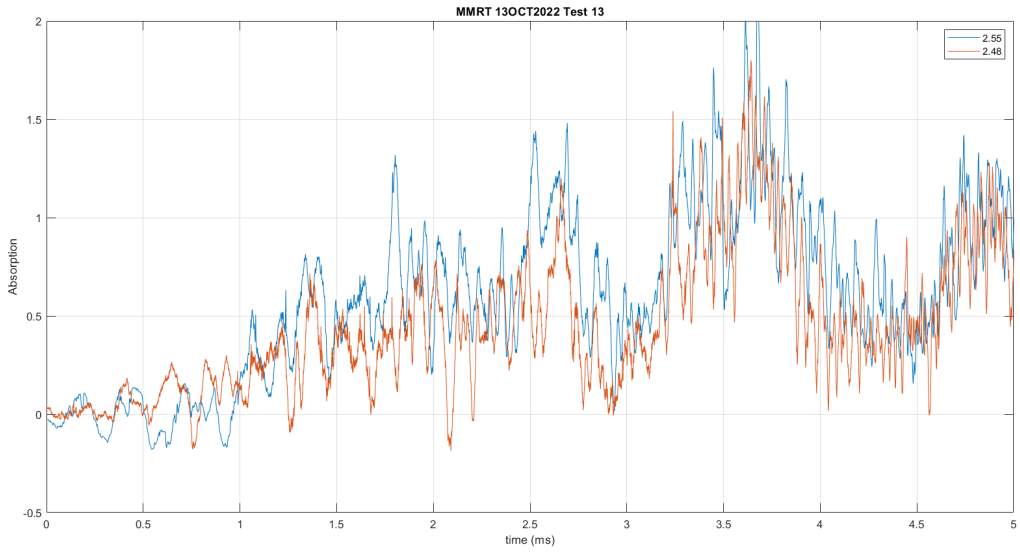

Figure 15: Absorbance trace of both H_2O lasers for test 13 of the experiment.

4.2 Temperature Results

The two figures above show a comparison between a test with no reactive material liner and a test with the reactive material liner inserted. The 13th test used a 0.13 lbs. reactive liner with explosive A, while the 10th test used explosive B with an inert liner. Based on the data, the reactive material liner and explosive A seemed to have improved the blast temperature significantly. Without these, the 2.48 µm laser minimum temperature for absorption was not reached. This means that with the current data, the temperature and species concentration cannot be determined for the tests without the reactive liner. Therefore, further testing will be required to measure these scenarios.

The laser system measured a temperature of approximately 1100 K with some fluctuations at the location of the probe. This led to the presented water concentration in Figure 17. The water concentration seems to increase steadily throughout the experiment. This behavior is expected, as more species will form with time after the initial detonation. There are some dips in the

concentration, but this is believed to be from vibrations of the blast steering the beams into better alignment. The nature of this experiment introduced a lot of particles and soot formation on the windows of the probe. The blast wave is believed to be the main contributor to these noises. Due to this, there is a time limit for how much data can be recorded before the particles as well as soot from the blast wave completely block the lasers. After 6 milliseconds, the laser beams start to experience significant attenuation.

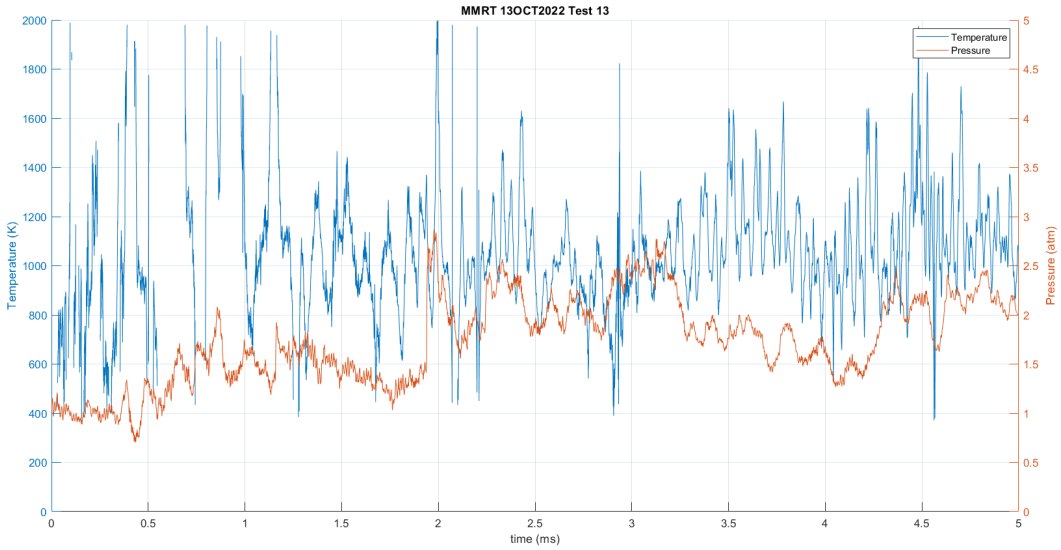

Figure 16: Plot of the temperature and pressure traces for test 13.

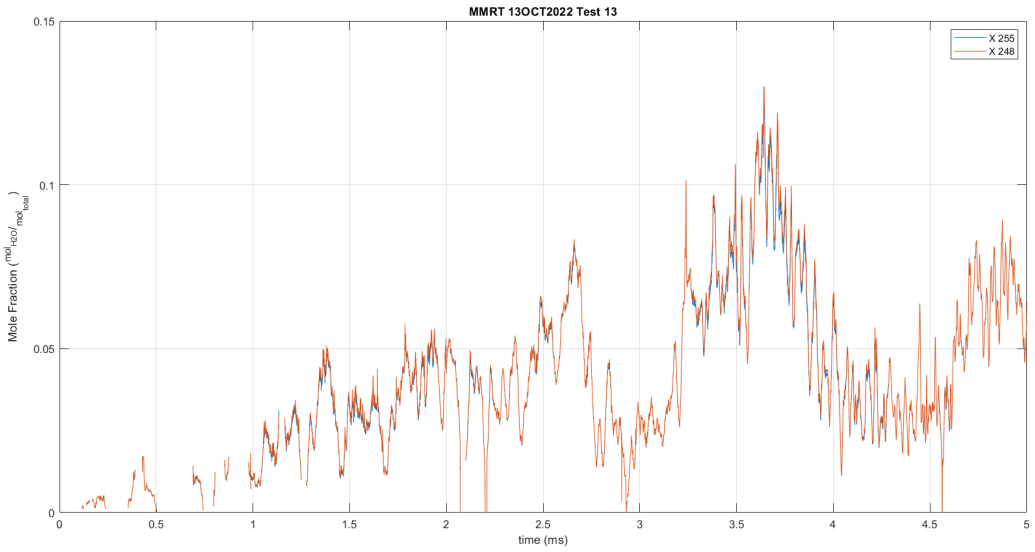

Figure 17: Plot of the species concentration as a function of time for test 13.

4.3 Future Remarks

The diagnostic system will need to be improved to account for the noises from vibrations. Perhaps adding a dampening system on the optical components inside the probe will sufficiently mitigate these noises. The issue with the laser's seemly inability to absorb with the inert liner tests will also need to be resolved. More data needs to be collected to determine if the lasers themselves are the issues or if this is some phenomenon that occurs in the blast. It is possible that the issue lies with the power output of the laser, as they are class 1M lasers. Although, this possibility can be countered by the 2.55 µm laser's signal. Both lasers are the exact same type of laser, so if there is a power issue with the 2.48 µm laser, this should also be the case for the 2.55 µm laser. Seeing that there is absorbance for the 2.55 µm laser with both the inert and the reactive material liner, means that the max power output of the lasers is not a significant issue. There is likely a difference in blast propagation and temperature between the different explosives, and inert and reactive liner

tests. Currently, we are not able to discern between the effects of these changing parameters, but we hope to accomplish this in the future.

CONCLUSIONS

The probe system seemed to have been designed well for this experiment. It was able to resolve several issues that occurred. Although, it was not able to mitigate the noises produced by the blast wave. There appears to be an effect from the blast resulting from the changes in explosives and reactive material liner. Since explosive A is designed for internal blast applications, it should provide better performance within the MMRT structure than explosive B. Both the explosive A and the reactive material liner are believed to have increased the maximum blast temperature. From the current data, the laser system was able to measure a temperature of approximately 1100 K for the blast with explosive A and 0.13 lbs. reactive material liner. This validates the feasibility of the diagnostic instrument.

For this first set of tests, we were not able to collect as much data as we initially expected. There were several changes and accommodations that had to be completed to integrate the diagnostic instrument and the probe into the MMRT structure. In order to prevent delays to the testing, the laser system integration had to be delayed for several tests. With the limited amount of obtained data, the exact effects of changing parameters such as explosive and liner cannot be concluded. There does seem to be a difference in temperature between the tests when comparing the absorption values of both lasers. However, with the current data, the exact difference in temperature is not conclusive. This is because, for some of the tests, it is believed that the minimum absorption temperature for the 2.48 μm laser was not reached. Without having the ability to compare the different blast temperatures and molar fractions of H_2O, no noteworthy conclusions about the HE and RM pairings can be drawn. More testing will be required to reach a conclusion. The diagnostic system also needs modifications to improve on some of the experience uncertainties such as vibrational noise.

LIST OF REFERENCES

[1] Lu, D., Wang, H., Lei, M., and Yu, Q., 2017, "Enhanced Initiation Behavior of Reactive Material Projectiles Impacting Covered Explosives," Propellants, Explosives, Pyrotechnics, 42(9), pp. 1117-1123.

[2] Rinkenbach, W. H., and Audrieth, L., 1945, "Modern military high explosives," Journal of Chemical Education, 22(11), p. 522.

[3] Das, A. K., Uddi, M., and Sung, C.-J., 2012, "Two-line thermometry and H2O measurement for reactive mixtures in rapid compression machine near 7.6 μm," Combustion and flame, 159(12), pp. 3493-3501.

[4] Baer, D. S., Nagali, V., Furlong, E. R., Hanson, R. K., and Newfield, M. E., 1996, "Scanned- and fixed-wavelength absorption diagnostics for combustion measurements using multiplexed diode lasers," AIAA Journal, 34(3), pp. 489-493.

[5] Rahman, R. K., Barak, S., Wagnon, S. W., Kukkadapu, G., Pitz, W. J., and Vasu, S. S., 2022, "Shock tube investigation of high-temperature, extremely-rich oxidation of several co-optima biofuels for spark-ignition engines," Combustion and Flame, 236, p. 111794.

[6] Greene, R., Khanal, N., Etienne, M., Thurmond, K., Taylor, B., Wilde, B., Lacina, D., and Vasu, S. S., 2022, "Detonation Afterburn Temperature and Species Characterization using Laser Absorption Spectroscopy inside a Blast Chamber," JANNAF June Meeting 2022, Paper No: 8241.

[7] Ninnemann, E., Pryor, O., Barak, S., Neupane, S., Loparo, Z., Laich, A., and Vasu, S. S., 2021, "Reflected shock-initiated ignition probed via simultaneous lateral and endwall high-speed imaging with a transparent, cylindrical test-section," Combustion and Flame, 224, pp. 43-53.

[8] Loparo, Z. E., Ninnemann, E., Ru, Q., Vodopyanov, K. L., and Vasu, S. S., 2020, "Broadband mid-infrared optical parametric oscillator for dynamic high-temperature multi-species measurements in reacting systems," Optics Letters, 45(2), pp. 491-494.

[9] Loparo, Z. E., Ninnemann, E., Thurmond, K., Laich, A., Azim, A., Lyakh, A., and Vasu, S. S., 2019, "Acousto-optically modulated quantum cascade laser for high-temperature reacting systems thermometry," Optics Letters, 44(6), pp. 1435-1438.

[10] Goldenstein, C. S., Almodóvar, C. A., Jeffries, J. B., Hanson, R. K., and Brophy, C. M., 2014, "High-bandwidth scanned-wavelength-modulation spectroscopy sensors for temperature and H2O in a rotating detonation engine," Measurement Science and Technology, 25(10), p. 105104.

[11] Rieker, G. B., 2009, Wavelength-modulation spectroscopy for measurements of gas temperature and concentration in harsh environments, Stanford University.

[12] Hanson, R. K., Spearrin, R. M., and Goldenstein, C. S., 2016, Spectroscopy and optical diagnostics for gases, Springer.

[13] Jorgensen, F., and Zuiderwyk, M., 1985, "Two-colour pyrometer measurement of the temperature of individual combusting particles," Journal of Physics E: Scientific Instruments, 18(6), p. 486.

[14] Gordon, I. E., Rothman, L. S., Hill, C., Kochanov, R. V., Tan, Y., Bernath, P. F., Birk, M., Boudon, V., Campargue, A., and Chance, K., 2017, "The HITRAN2016 molecular spectroscopic database," Journal of Quantitative Spectroscopy and Radiative Transfer, 203, pp. 3-69.

[15] Zhou, X., Liu, X., Jeffries, J. B., and Hanson, R., 2003, "Development of a sensor for temperature and water concentration in combustion gases using a single tunable diode laser," Measurement Science and Technology, 14(8), p. 1459.